Analysis of Heat-Affected Zone Cracking in Ni_3Al Alloy Welds by Computer Modeling of Thermal Stresses

A method was developed for analyzing heat-affected-zone cracking using computer-generated thermal stress profiles

BY M. L. SANTELLA, M. C. MAGUIRE AND S. A. DAVID

ABSTRACT. The welding behavior of a Ni_3Al alloy containing 0.1 at.-% boron and 0.5 at.-% hafnium was studied by making a series of electron beam welds on a 0.7-mm (0.03-in.) thick sheet of the alloy at speeds of 2.1 to 42.5 mm/s (0.08 to 1.7 in./s). The welds were free of cracks. Hot ductility testing showed that the Ni_3Al+Hf alloy had no measurable ductility above 800°C (1472°F). Unlike the behavior of previously studied Ni_3Al alloys containing 10 at.-% iron, the poor hot ductility response of the Ni_3Al+Hf alloy did not correlate with susceptibility to heat-affected-zone cracking. The inconsistency of the correlation between weldability and hot ductility for these boron-doped Ni_3Al alloys was resolved by modeling the transient thermal stresses that develop in the heat-affected zone during welding. A computer-aided analysis indicated that the susceptibility to heat-affected-zone cracking was a function of thermal conductivity as well as high-temperature strength and ductility. The thermal conductivity of the Ni_3Al+Hf alloy was higher than that of the Ni_3Al+Fe alloys, and this fact resulted in lower thermal stresses in the Ni_3Al+Hf alloy as a result of welding. The predicted thermal stresses in the Ni_3Al+Hf alloy never exceeded its yield strength, consequently high-temperature ductility was not an important factor in its resistance to heat-affected-zone cracking. The predicted thermal stresses in the Ni_3Al+Fe alloys, however, did exceed their yield strengths at high temperature. The Ni_3Al+Fe+0.10B alloy had ductility of 15 to 20% between 1100°C (2012°F) and the melting point and was resistant to heat-affected-zone cracking, but the Ni_3Al+Fe+0.24B alloy had no high-temperature ductility above 800°C and showed extensive heat-affected-zone cracking. For all three alloys, predictions based on analysis of welding-induced thermal stresses agreed with the observed cracking behavior.

M. L. SANTELLA and S. A. DAVID are with Oak Ridge National Laboratory, Metals and Ceramics Division, Oak Ridge, Tenn. M. C. MAGUIRE is with the Center for Welding Research, Colorado School of Mines, Golden, Colo.

This paper is based in part on a paper titled "An Analysis of Heat-Affected Zone Cracking in Ni_3Al Alloys," presented at the 67th Annual AWS Meeting, held April 13–18, 1986, in Atlanta, Ga.

Introduction

Polycrystalline Ni_3Al and many of its alloys can be made ductile by microalloying with boron (Refs. 1, 2), and because of the unusual mechanical properties of Ni_3Al alloys, there is interest in their development for structural applications. Good weldability is a desirable feature of structural materials and it is one of the properties being addressed in development of Ni_3Al alloys. Early work in this area (Ref. 3) described the effect of boron on the weldability of Ni_3Al, discussed the microstructure of welds in Ni_3Al containing iron additions, and showed that Ni_3Al+Fe alloys could be welded, but were susceptible to intergranular cracking in the heat-affected zone (HAZ).

KEY WORDS

Heat-Affected Zone
HAZ Cracking
Ni_3Al Alloy Welds
Computer Modeling
Thermal Stresses
Thermal Stress Model
Stress Profiles
Electron Beam Welding
Transient Stresses
Longitudinal Stresses

Subsequent studies (Refs. 4, 5) of the welding behavior of the Ni_3Al+Fe alloys correlated boron concentration with the resistance to HAZ cracking. The microstructure of HAZ cracks indicated that they were intergranular in nature, and that they formed in the solid state. It was suggested (Ref. 4) that the cracks were caused by the longitudinal thermal stresses induced during welding, and weakening of the grain boundaries at elevated temperature. Later, the weldability of the Ni_3Al+Fe alloys was correlated with their hot ductility (Ref. 5). It was shown that an alloy containing 200-wppm boron was much more resistant to HAZ cracking than was an alloy containing 500-wppm boron. Also, the lower boron alloy was found to have relatively good high-temperature ductility. Based on a dislocation pile-up model, it was concluded that the lower boron alloy had higher grain boundary strength at high temperatures, which accounted for its better weldability and ductility.

The primary aim of this paper is to discuss the role of thermally induced stresses on the HAZ cracking of boron-doped Ni_3Al alloys in more detail. New weldability and hot-ductility data for a Ni_3Al+Hf alloy are presented. In addition, it will be shown that for the combined results of the Ni_3Al+Fe and Ni_3Al+Hf alloys, a consistent correlation between HAZ cracking and hot ductility cannot be made. To address this inconsistency, a computer model developed by Masubuchi and coworkers (Refs. 6, 7) that can predict thermal stress distributions around weld puddles was used to analyze the welding and ductility data. This approach permitted a comparison to be made between thermally induced stresses and yield strengths, and when coupled with hot-ductility data, a coherent picture of the probable causes of HAZ cracking in boron-doped Ni_3Al alloys was obtained. Our analysis indicated that yield strength, ductility and thermal con-

Table 1—Alloy Compositions (at.-%)

Alloy Identification	Composition			
	Ni	Al	B	Others
IC-50	75.9	23.5	0.1	0.5Hf
IC-25	69.9	18.9	0.24	10.0Fe+0.5Ti +0.5Mn
IC-103	70.0	18.9	0.1	10.0Fe+0.5Ti +0.5Mn

ductivity are important factors in determining the susceptibility to HAZ cracking, and that alloys with poor high-temperature ductility can be resistant to HAZ cracking if their thermal conductivity is relatively high.

Materials and Experimental Details

Welding Behavior

The nominal compositions of the alloys considered in this study are listed in Table 1. The Ni_3Al+Fe Alloys IC-25 and IC-103 were prepared as 500-g (17.5-oz) arc-melted ingots and the Ni_3Al+Hf Alloy IC-50 was prepared as a 22.5-kg (49.5-lb) arc-melted ingot. All three alloys were made into sheet by cold rolling with repeated annealing, and were single phase with the fully ordered $L1_2$ crystal structure after final annealing. The recrystallized grain sizes of finished sheets were ASTM 8 (20 μm) in each case.

The details of welding and hot-ductility testing the Ni_3Al Alloys IC-25 and IC-103 have already been described (Ref. 5). The welding behavior of IC-50 was similarly assessed by making a series of full-penetration autogenous electron beam (EB) welds on the 0.7-mm sheet. Welding was done in a Leybold-Heraeus 15-kW machine at speeds between 0.9 and 63.5 mm/s (0.04 and 2.5 in./s). The welding coupons were held in a heavy copper fixture. Examination for cracks was done at 100X on as-welded surfaces. The occurrence of cracks was verified on metallographically prepared specimens. Hot-ductility testing of IC-50 was done on a Gleeble 1500 thermomechanical simulator at a nominal strain rate of 3 mm/s. The test procedure and specimen configuration were identical to those used for IC-25 and IC-103 (Ref. 5).

Computer Modeling

Thermal Profile Calculations

Two programs were used to model thermal and mechanical behavior during the welding process. Both programs were written in the FORTRAN programming language and were run on a PDP-10 computer. The first program determined temperature profiles based on welding parameters and physical properties of the Ni_3Al alloys. These data, coupled with mechanical property information, were then used for stress and strain determination in the second program. Both programs were developed by Masubuchi and coworkers (Refs. 6, 7) for determination of thermal stresses during welding, and are particularly well suited for use in analyzing thin sheet material because they treat the heat-flow problem two-dimensionally, ignoring thickness effects. Both programs divide the welding process into a set of time steps with the heat source at some fixed time. Modifications to the original programs were made to describe bead-on-plate autogenous welding rather than butt joint welding conditions, and to simplify changing the distance between sampling points for numerical integration of thermal stress profiles. Temperature distributions were calculated using a linearized heat-flow equation for a moving line source after Rosenthal (Ref. 8). This equation takes the form of

$$\theta = [q/(2\pi\Gamma)] \times [\exp(-v\phi/2k)] \times K_o(vr/2k) \quad (1)$$

where,

θ = temperature change
$k = \Gamma/(c_p \cdot \rho)$ = thermal diffusivity
c_p = specific heat
ρ = density
Γ = thermal conductivity
t = time
v = speed of the moving heat source
x = coordinate in a fixed system
$\phi = x - vt$, coordinate in a moving system
q = net-heat-input per plate thickness
$K_o(z)$ = modified Bessel function of the second kind and zero order
$r = (\phi^2 + y^2)^{1/2}$

The temperature calculation program required input information on welding parameters and three physical properties: density, heat capacity and thermal conductivity. Changes in these material properties with temperature were accommodated by an iterative solution scheme to the equation for temperature change, θ. Each solution matches the calculated temperature with the physical property at that temperature. Thus, the program requires that the physical properties be known in the temperature range from ambient temperature to the melting point. The variations of density, heat capacity and thermal conductivity are discussed in the Appendix.

The welding parameters for the calculation were selected to produce weld bead widths in the range of 0.4 to 4 mm (0.02 to 0.2 in.) because this corresponded to the bead widths observed for the EB welds. Overall, the heat-input values used for the calculations were realistic approximations of actual values. At a particular welding speed, the heat input required of the Ni_3Al+Hf alloy was higher than that required of the Ni_3Al+Fe alloys for a given bead width, also in agreement with our observations of welding behavior.

Thermal Stress Calculations

The thermal stresses generated in the HAZ by strains parallel to the welding direction, which resulted from thermal gradients surrounding the heat source, were then calculated by the second program based on the work of Tall (Ref. 9). Thermal stresses normal to the welding direction are considered to be negligible (Refs. 6, 7) by comparison and are ignored in the calculations. Data for elastic modulus, yield strength, coefficient of thermal expansion and strain-hardening behavior over the temperature range from ambient to the melting temperature were used to calculate strains in an iterative manner similar to the temperature program. The input physical and mechanical properties data are also discussed in the Appendix. Once strains were evaluated, the corresponding stress was calculated by assuming the material exhibited elastic and linear plastic behavior.

Strain calculations were performed by dividing the plate into elements normal to the welding direction with each element having a thickness equal to the product of the time increment and the welding speed. Ten positions perpendicular to the weld direction were selected in each element at which strains and stresses were calculated. The first calculation was done ahead of the heat source where the plate contained no strain. The initial stress distribution was calculated by considering only thermal contraction or expansion. Each subsequent calculation was based on thermal strains as well as the strain from the previous element. In this fashion, the mechanical strain at each position was determined, and the corresponding stress was calculated. Typical output from the programs consisted of calculated longitudinal thermal stress, σ_T, yield or fracture strength of the alloy, σ_M, temperature, time and distance from the arc tabulated for a grid of points lying in the plane of the sheet. Most interest was in the HAZ material immediately adjacent to the fusion line, so data points were concentrated in that region. A spline function was used for plotting σ_T and σ_M against distance and temperature.

Results

The EB welds made on IC-50 were free of cracks except for termination crater cracks in the welds made at 21.2 and 42.5 mm/s (0.8 and 1.7 in.). The data for IC-50 are shown in Fig. 1 with previous results (Refs. 4, 5) for EB welds made on Ni_3Al+Fe alloys. Examination of metallo-

graphically prepared samples confirmed that even the welds made in IC-50 at 42.5 mm/s were free of HAZ cracks. Figure 1 shows that only IC-25 had a tendency for HAZ cracking, and that this tendency increased with welding speed. For the data of Fig. 1, an increase of welding speed corresponded to a decrease of heat input. At a particular welding speed and bead width, the product of voltage and current was typically 10 to 30% higher for the Ni_3Al+Hf alloys than it was for the Ni_3Al+Fe alloys. Table 2 shows welding parameters actually used.

Based on previous analysis of the Ni_3Al+Fe alloys (Refs. 10–12), and on the observation that IC-50 was resistant to HAZ cracking, as shown in Fig. 1, it was anticipated that IC-50 would have measurable high-temperature ductility like the Ni_3Al+Fe Alloy IC-103. However, IC-50 had no ductility above 800°C and, in this respect, mirrored the behavior of IC-25. The tensile ductility of IC-50 is compared to that of the Ni_3Al+Fe alloys (Ref. 5) in Fig. 2, which shows that between 600° and 800°C (1112° and 1472°F) the ductilities of all three alloys decreased sharply to values near zero. Above 800°C only IC-103 recovered some ductility, and this occurred between about 1100°C and its melting point. Thus, while the weldability of the Ni_3Al+Fe Alloys IC-25 and IC-103 correlated very well with hot ductility, the behavior of the Ni_3Al+Hf alloy and differences between it and the Ni_3Al+Fe alloys could not be similarly explained.

The IC-50 hot-ductility specimens were examined in a scanning electron microscope (SEM) after testing. The appearance of a specimen tested at 700°C (1292°F) is shown in Fig. 3A, and is typical of the fracture appearance of specimens tested in the range of 600° to 800°C. The fracture mode was a mixture of intergranular and transgranular, and is consistent with a material exhibiting limited tensile ductility. The appearance of a specimen tested at 1200°C (2192°F) is shown in Fig. 3B. In this case, failure occurred by intergranular fracture with no measurable tensile ductility. The appearance of this specimen typified that of specimens tested from 800°C to 1300°C (1472° to 2372°F).

The inconsistency of the correlation between hot ductility and weldability for the Ni_3Al alloys led to selection of an alternate method for analyzing their behavior. The Masubuchi (Refs. 6, 7) programs were chosen because they describe the effects of differences in physical properties and mechanical properties other than ductility on thermal stresses induced by welding. Thermal stresses calculated by the programs were compared to the yield strength and graphically represented in two cases, shown in Fig. 4. The upper plot in Fig. 4 represents longitudinal thermal stresses, σ_T, as a

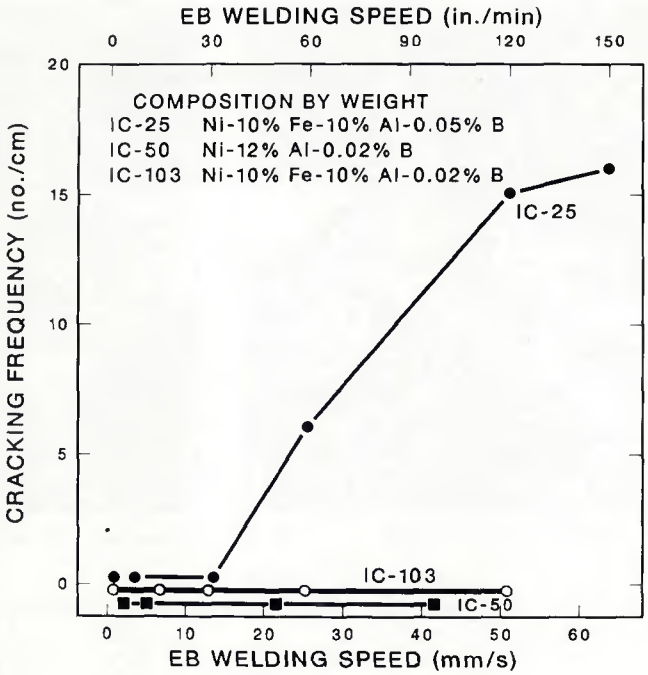

Fig. 1—Plot of heat-affected-zone cracking frequency versus electron beam welding speed for boron-doped Ni_3Al+Fe and Ni_3Al+Hf alloys

Table 2—Parameters for Autogenous EB Welds on 0.7-mm-thick Sheet of Ni_3Al Alloys

Alloy Identification	Welding Speed (mm/s)	Current (mA)	Voltage (kV)	Heat Input (J/mm)
IC-25/IC-103	0.9	1.4	60	99.2
(Ni_3Al+Fe)	1.7	2.0	60	70.2
	3.4	2.5	60	44.3
	6.8	3.0	60	26.6
	12.7	3.4	90	24.1
	25.4	4.1	100	16.1
	50.8	5.0	100	9.8
	63.5	6.0	100	9.4
IC-50	2.1	2.0	60	56.6
(Ni_3Al+Hf)	4.2	2.5	60	35.5
	10.6	4.5	60	25.5
	21.2	6.8	60	19.2
	42.3	6.5	95	14.6

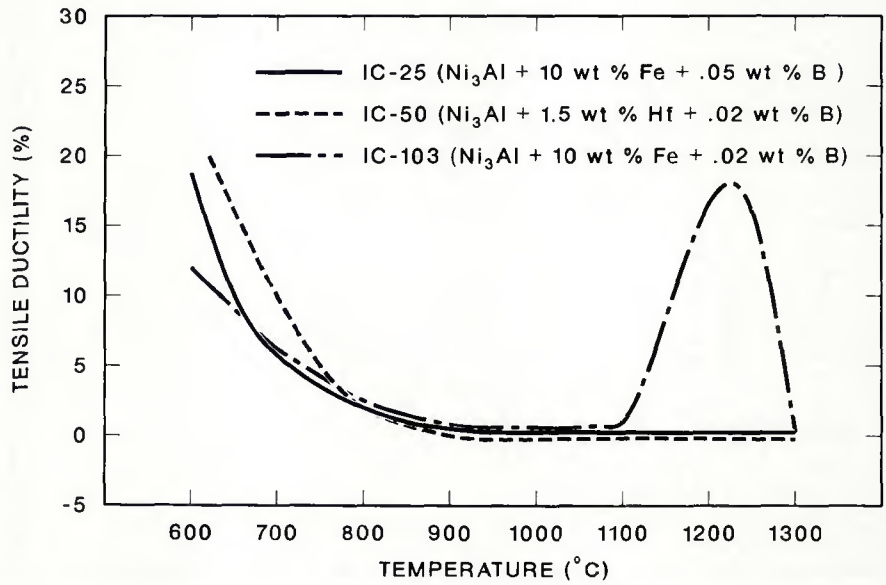

Fig. 2—Plot of tensile ductility versus temperature for boron-doped Ni_3Al+Fe and Ni_3Al+Hf alloys tested in air at 3.2/s

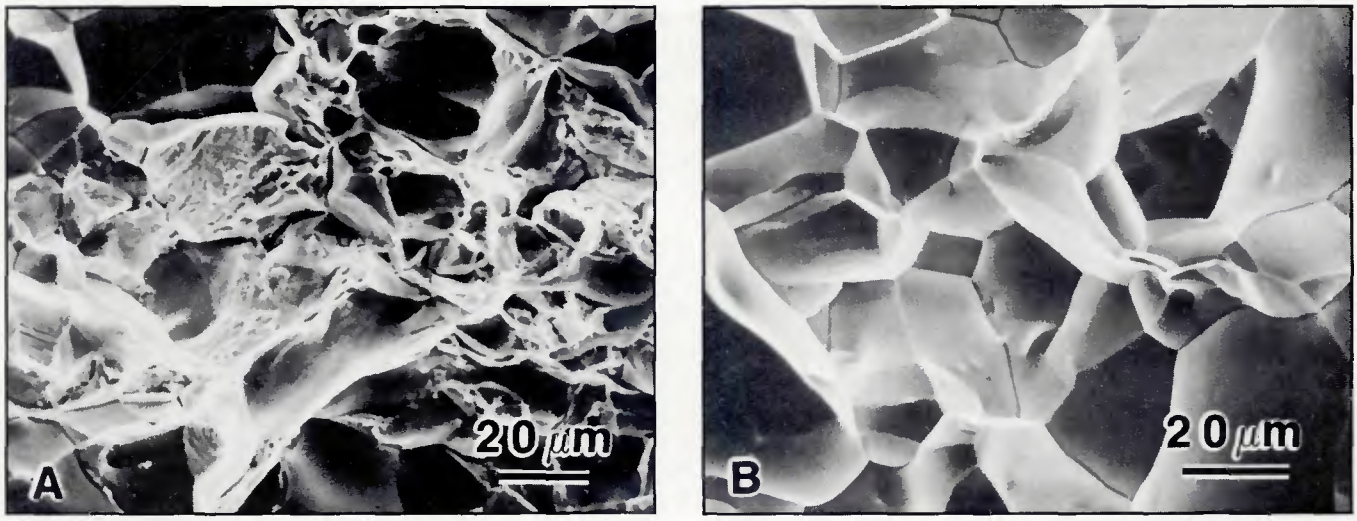

Fig. 3—Scanning electron micrographs of fracture surfaces from hot-ductility specimens of Ni_3Al+Hf Alloy IC-50 tested at: A—700°C; B—1200°C

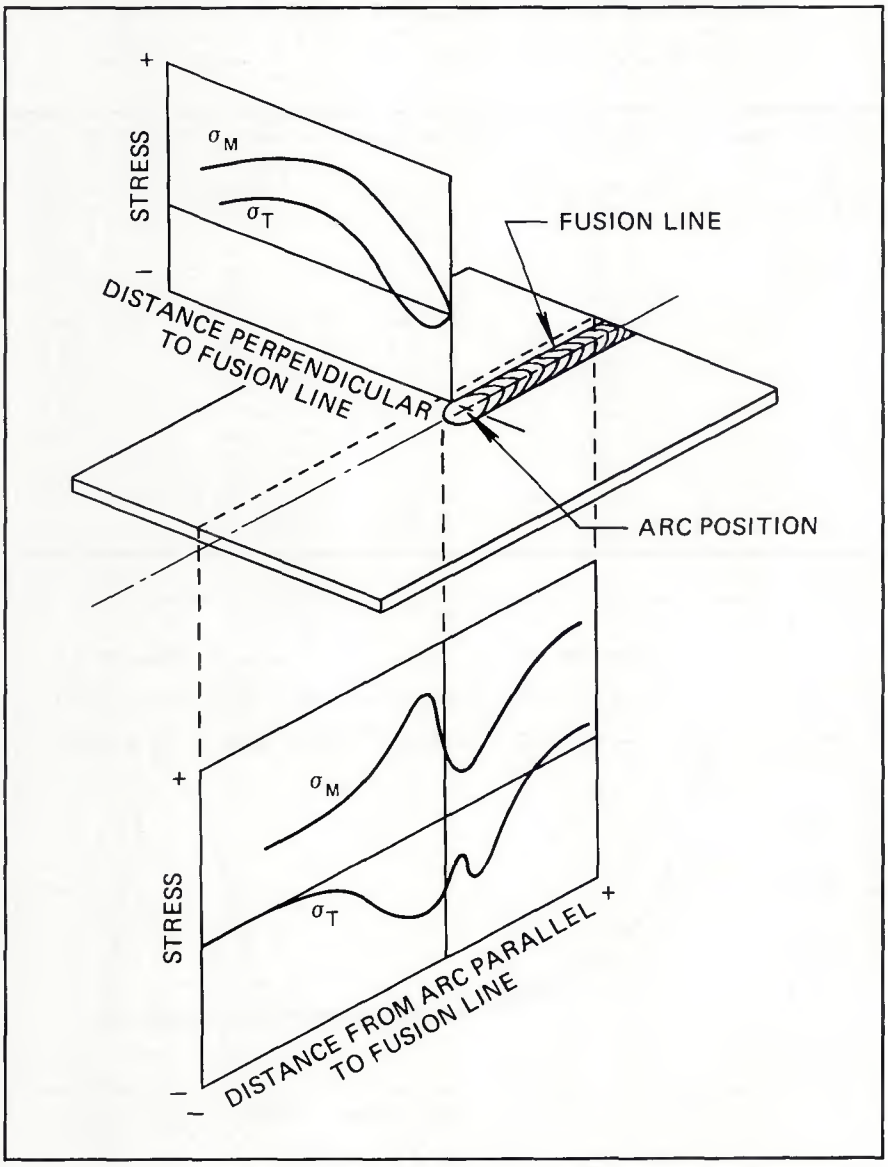

Fig. 4—Schematic representation of the types and orientation of stress plots generated by computer programming. σ_T = Induced longitudinal thermal stress; σ_M = yield strength

function of distance along a line perpendicular to the welding direction and originating at the fusion line. The distance of a point from the fusion line defined its temperature, and these data were subsequently plotted against temperature to aid in interpretation. The lower plot in Fig. 4 shows σ_T as a function of distance from the heat source along a line in the HAZ parallel to the fusion line.

A plot of the variation of σ_T with temperature for the Ni_3Al+Fe alloys is shown in Fig. 5. The experimentally determined yield strength σ_M is also plotted in Fig. 5 for comparison. The stress profiles shown extend into the base material along a line perpendicular to the weld fusion line. The maximum temperature occurs at the fusion line and decreases with distance from this point. Figure 5 indicates that for the Ni_3Al+Fe alloys σ_M decreases from about $0.5T_m$ up to the melting point, while the induced stress σ_T increases from about $0.7T_m$ to $0.95T_m$ and then falls to zero at the fusion line. The stress induced by welding is predicted to exceed the yield strength at about $0.9T_m$, *i.e.*, at a point in the HAZ very near the fusion line. Alloys with this type of behavior would be expected to have low resistance to HAZ cracking unless they could accommodate the induced stresses by plastic flow.

Figure 6 shows a similar plot of the variation of σ_T and σ_M with temperature for IC-50. In this case, the induced stress never exceeded the yield strength. This type of behavior is indicative of high resistance to HAZ cracking. Furthermore, Fig. 6 indicates that the amount of high-temperature ductility the alloy had would be unimportant because the induced stresses remained below the yield strength. The data shown in Figs. 5 and 6 were taken from the time segment 0.2 s behind the moving arc because this was the time increment when the maximum

stress induced in the HAZ occurred. The temperature increments used were the smallest ones that could be used with the mathematical functions employed by the program, and corresponded to distance increments on the order of 100 μm near the fusion zone. It should also be noted that the yield strength σ_M for these materials was taken to be the fracture strength over the temperature range where there was no ductility.

The effect of heat input on the induced thermal stresses were also examined. For both types of alloys, calculations were done for increases and decreases in heat input values, corresponding respectively to decreases and increases in welding speed. Figure 1 shows that IC-25 begins to crack at welding speeds greater than 12.7 mm/s (0.5 in./s), which corresponds to a heat-input value of 24.1 J/min (612 J/in.). Reducing the heat input to 24 J/mm corresponded to a critical cracking threshold in the computer analysis as well. The effect of variations in heat input on the induced stresses in the Ni_3Al+Fe alloy is shown in Fig. 7 where thermal stress data are plotted as a function of longitudinal distance from the arc. Figure 7A shows that for a heat input of 16 J/mm (160 J/in.), the σ_T sharply exceeded σ_M just as the heat source passed a fixed reference point. This situation would produce HAZ cracking in IC-25 because it occurs in a temperature range where the material has no ductility. Increasing the heat input to 24 J/mm (Fig. 7B) reduced the induced thermal stresses in the region directly behind the arc, but they still exceeded the yield strength at a temperature (~950°C/1742°F) where IC-25 had no ductility. To resist HAZ cracking, the crossover point of σ_T and σ_M would have to occur at still lower temperatures where some recovery of ductility would be possible. Figure 7C shows that for a heat input of 27 J/mm, σ_T never exceeded σ_M. The position of maximum stress induced in the HAZ during welding was generally no more than 0.2 mm (0.008 in.) from fusion line.

Similar calculations were made for welds in IC-50, and an example of the effect of decreasing the heat input from 35 to 15 J/mm (889 to 381 J/in.) on σ_T is in Fig. 8. For this alloy, the heat input could not be decreased enough to cause σ_T to exceed σ_M in a temperature range where the ductility was negligible. This behavior suggested IC-50 should be relatively resistant to HAZ cracking.

Each individual curve plotted in Figs. 7 and 8 contains 21 data points, some of which were omitted for the sake of visual clarity.

Discussion

In a previous study (Ref. 4), it was suggested that the HAZ cracks that occurred in the high-speed welds in IC-25 were caused by induced tensile stresses in the HAZ. Analysis of welded and hot-ductility specimens indicated that the grain boundary cohesive strength of IC-25 was lower than its yield strength at elevated temperatures and responsible for its brittle behavior. The resistance of IC-103 to HAZ cracking was explained as being due to the recovery of ductility at high temperature, thereby allowing the accommodation of thermal stresses produced during welding by plastic flow. The response of an alloy to hot-ductility testing has often been correlated to welding behavior (Refs. 10–12), and the results of the work on the boron-doped Ni_3Al+Fe alloys appeared to be a classic case of cracking susceptibility being related to loss of high-temperature ductility. However, when the weldability of IC-50 could not be correlated with ductility, it was decided to examine this problem more closely by analyzing the effects of thermal stress on HAZ cracking.

The origins of the thermal stresses produced during welding, and how this problem has been addressed by various investigators, was discussed in detail by Masubuchi (Ref. 13). Based on his review, it was decided to adapt an analysis developed by Masubuchi and coworkers (Refs. 6, 7) to the problem of describing induced thermal stresses in Ni_3Al alloys and how they relate to HAZ cracking. Because the calculation ignores tempera-

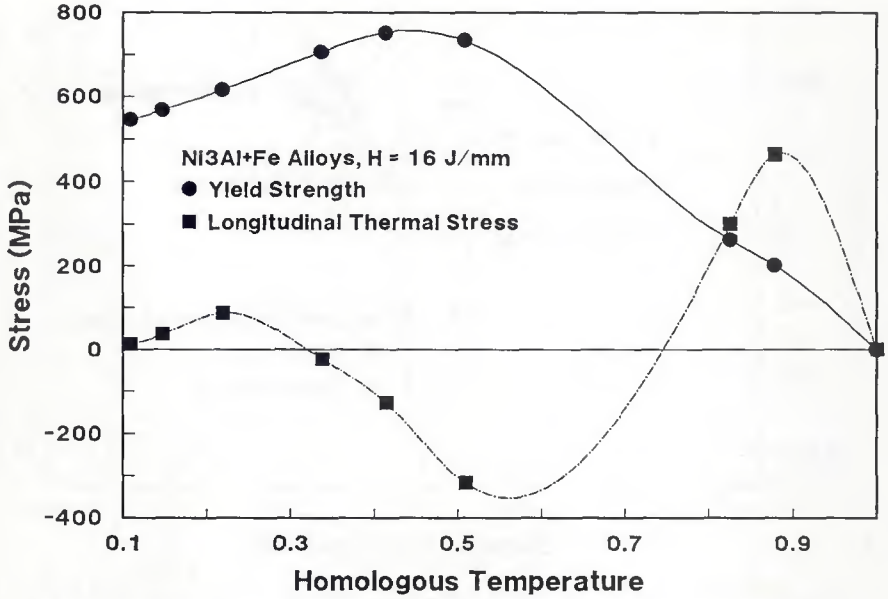

Fig. 5 — Plot of induced thermal stress σ_T, and yield strength σ_M versus temperature for Ni_3Al+Fe Alloys IC-25 and IC-103

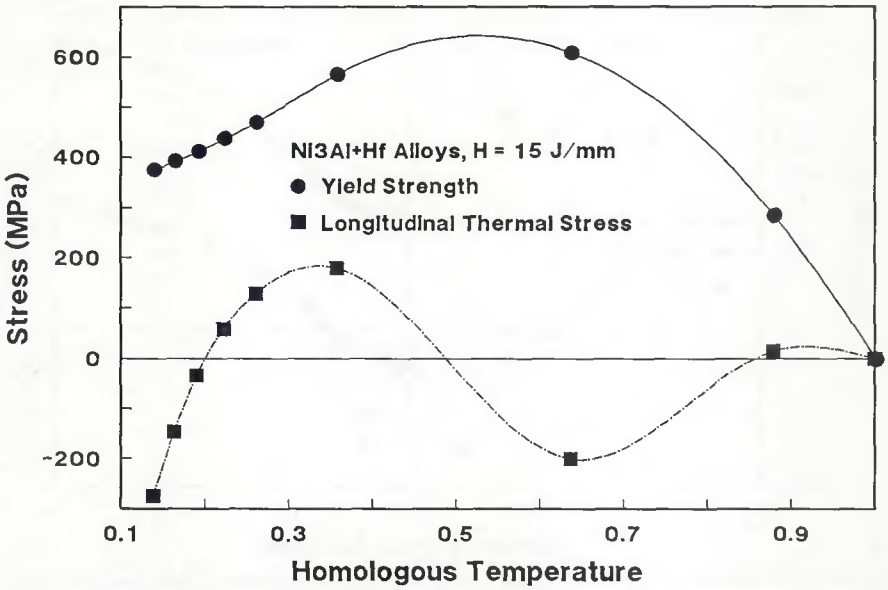

Fig. 6 — Plot of induced thermal stress σ_T, and yield strength σ_M versus temperature for Ni_3Al+Hf Alloy IC-50

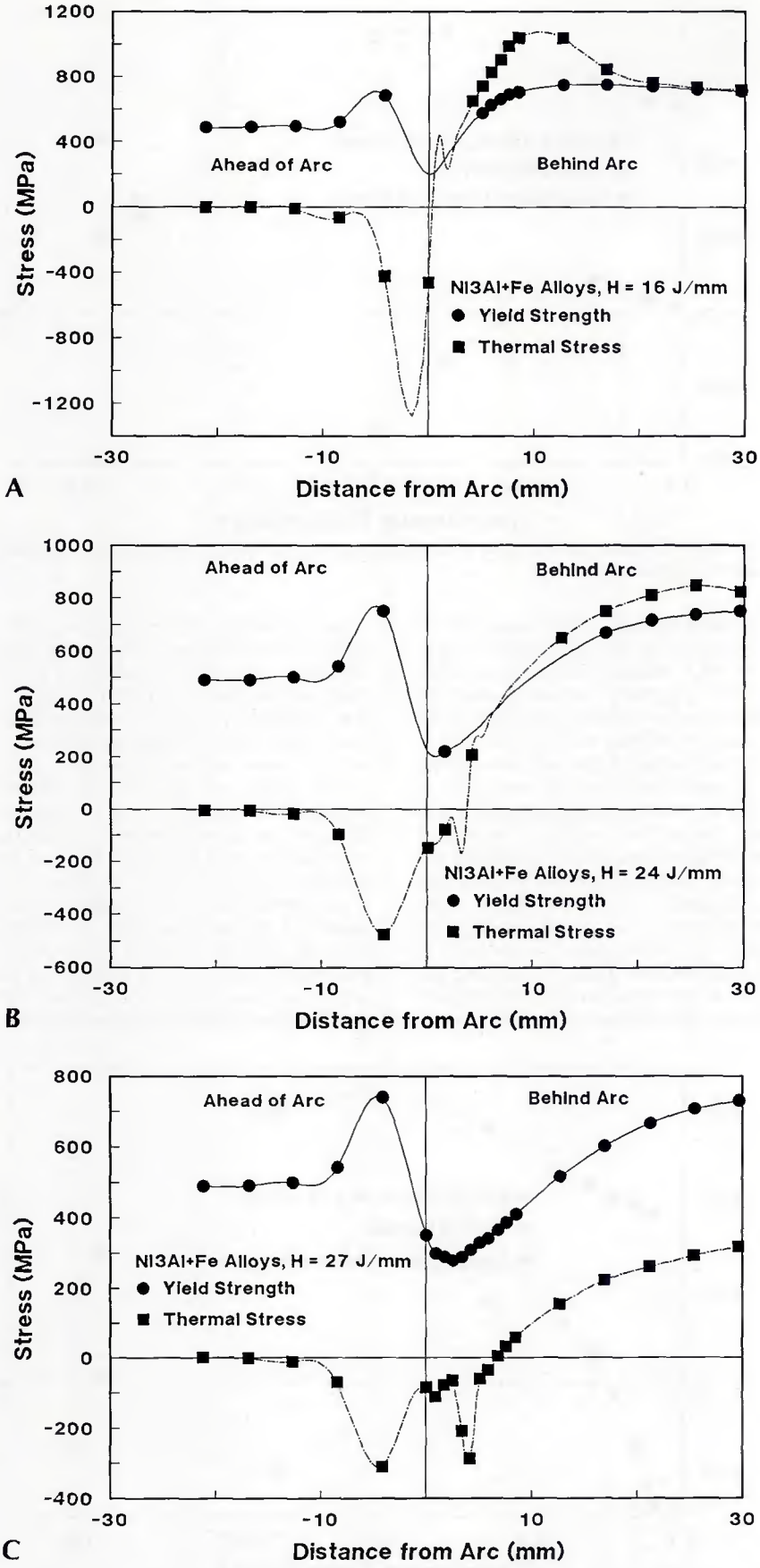

Fig. 7 — Plot of induced thermal stress σ_T, and yield strength σ_M versus longitudinal distance from the heat source for Ni_3Al+Fe alloys at heat input values of: A — 16 J/mm; B — 24 J/mm; C — 27 J/mm. Some data points were omitted for clarity

ture changes in the through-thickness direction, it closely approximates autogenous welding of large, thin plates. The welding coupons used for the present experiments were not extremely large, but they were held between large copper grips which were effective heat sinks. Thus, our experimental conditions were matched closely with the thermal conditions assumed by the computer program. The agreement between the heat-input values used for welding and those used for calculation also attests to the accuracy of the program in representing the experimental conditions.

Once the temperature profiles about the arc are determined, the Masubuchi analysis (Refs. 6, 7) calculates only the longitudinal stresses and assumes that stresses perpendicular to the weld axis as well as shear stresses are zero. Examination of HAZ cracks in IC-25 showed that they typically occurred near the fusion line and extended into the base material in a direction perpendicular to the fusion line (Refs. 3, 4). The orientation of the HAZ cracks suggested that longitudinal stresses, *i.e.*, stresses acting in the same direction as the welding direction, were responsible for crack formation (Ref. 4). Therefore, characteristic HAZ cracking in Ni_3Al alloys is also compatible for treatment with the Masubuchi analysis.

The variation of thermally induced stress with temperature along a line perpendicular to the axis of a weld in a Ni_3Al+Fe alloy (Fig. 5) was calculated for a heat-input value of 16 J/mm. This corresponds to a welding speed of 25.4 mm/s (1 in./s), and was the speed at which HAZ cracks were first observed in IC-25. The temperature range over which the induced stress is predicted to exceed the yield strength of the Ni_3Al+Fe alloys is approximately 1180°C (2156°F) to the melting point, about 1320°C (2408°F). In terms of distance, this occurs within about 400 μm of the fusion line. The IC-25 alloy had no ductility over the temperature range where the yield strength was exceeded, and thus would likely crack in the HAZ near the fusion line. On the other hand, IC-103 had very good ductility between about 1100°C and the melting temperature, and can accommodate the thermally induced stresses by local plastic flow. Because it has high-temperature ductility, IC-103 would not be expected to crack in the HAZ under the same conditions as IC-25.

Decreasing the welding speed for the Ni_3Al+Fe alloys resulted in welds that were free of HAZ cracks — Fig. 1. Decreasing the welding speed corresponded to increasing the heat input and the effect of this change in welding conditions on thermal stresses is illustrated in Fig. 7. Increasing the heat input from 16 to 24 J/mm resulted in conditions where

the thermally induced stresses slightly exceeded the yield strength of the Ni_3Al+Fe alloys in the HAZ. This heat-input condition is close to the highest welding speed (12.7 mm/s) at which crack-free welds were obtained in the IC-25 alloy. Figure 7 also shows that a further increase from 24 to 27 J/mm (610 to 686 J/in.) should suppress HAZ cracking. The behavior predicted by the Masubuchi analysis is, therefore, in excellent agreement with experimental observations of HAZ cracking in the Ni_3Al+Fe alloys.

The observed welding behavior of IC-50 was also in agreement with the predictions of the Masubuchi analysis. The IC-50 alloy was very resistant to HAZ cracking as shown in Fig. 1. The IC-50 alloy had no ductility above about 800°C, but the thermal stresses induced in the HAZ of this alloy by welding (Fig. 8) were predicted to be below the yield strength. The data presented in Fig. 8A correspond to a heat-input value of 15 J/mm (381 J/in.), or a welding speed near 42 mm/s (1.7 in./s). A decrease of heat input to 35 J/mm (4.2 mm/s) decreased the difference between the maximum induced thermal stress and the yield strength, but the yield strength was still not exceeded at a temperature high enough to cause loss of ductility. Based on the computer-aided analysis, IC-50 would be expected to be very resistant to HAZ cracking.

The combination of experimental observations of welding behavior and computer-aided analysis of the thermal stresses induced by welding suggest that the occurrence of HAZ cracking in the Ni_3Al alloys can be described by the following three relationships between yield or fracture strength, σ_M, induced longitudinal thermal stress, σ_T, and high-temperature ductility:

1) $\sigma_T > \sigma_M$, *no ductility*—In this case, because the yield strength is exceeded and the material cannot accommodate the high induced thermal stresses by plastic flow, brittle fracture occurs in the HAZ. The Alloy IC-25 exhibited this type of behavior.

2) $\sigma_T > \sigma_M$, *some ductility*—Even though the yield strength is exceeded, local plastic flow permits accommodation of the induced thermal stresses and HAZ cracking is unlikely. The behavior of IC-103 is an example of this case.

3) $\sigma_T < \sigma_M$—HAZ cracking does not occur for this condition because thermal stresses never exceed the yield strength of the material. Under this condition, whether or not a material has good high-temperature ductility is unimportant. The Alloy IC-50 illustrates this behavior.

The analysis of HAZ cracking presented here is similar to one proposed by Yeniscavich (Ref. 14), but treats the problem in a quantitative manner. Furthermore, it is expected that our analysis and the relationships above are general, and therefore, could be applied to the study of other alloys that are susceptible to HAZ cracking.

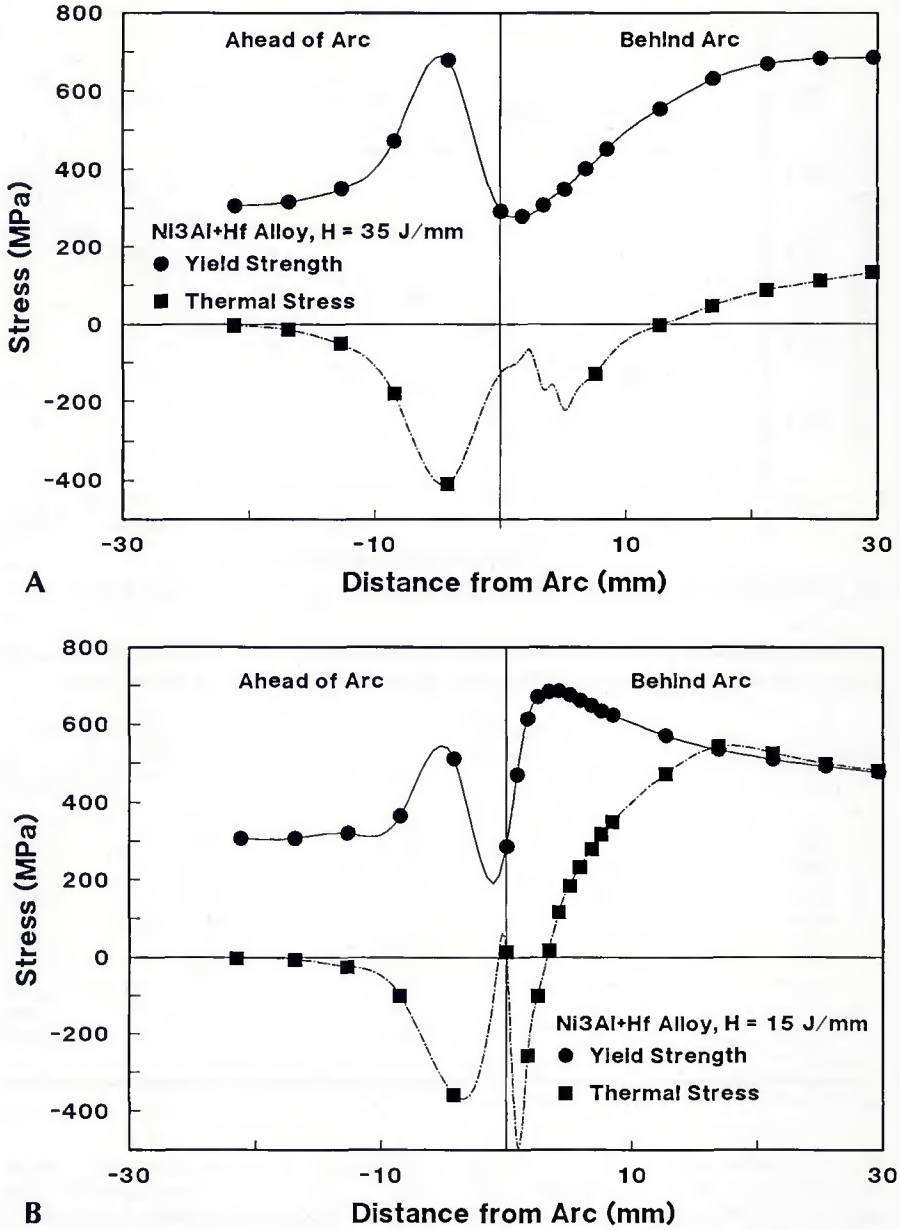

Fig. 8 — Plot of induced thermal stress σ_T, and yield strength σ_M versus longitudinal distance from the heat source for the Ni_3Al+Hf alloy at heat input values of: A — 35 J/mm; B — 15 J/mm. Some data points were omitted for clarity

The reason IC-50 had such good weldability when it had very little or no high-temperature ductility is that its thermal conductivity was relatively high, as shown in the Appendix. The IC-50 alloy is a good conductor of heat. This minimizes the effects of the thermal stresses induced by welding because heating becomes less localized in the region of the weld fusion zone and thermal gradients in the unmelted base metal are relatively low. On the other hand, IC-25 is a much worse conductor, and therefore, experiences considerably higher thermal stresses. The better conductivity of IC-50 is directly related to the lower level of alloying additions in this alloy (0.5 at.-%) compared to IC-25 (10.0 at.-%). The high-temperature strength of IC-50 is higher than that of the Ni_3Al+Fe alloys, as shown in the Appendix, and while this contributes to its good resistance to HAZ cracking, thermal conductivity is a much more important factor. The computer analysis, therefore, resulted in additional insight into the problem of HAZ cracking of the Ni_3Al alloys, and provided a reasonable explanation of the inconsistency of the correlation between weldability and hot ductility.

While the computer-aided analysis is general and relatively straightforward, the correlation of the hot ductility of

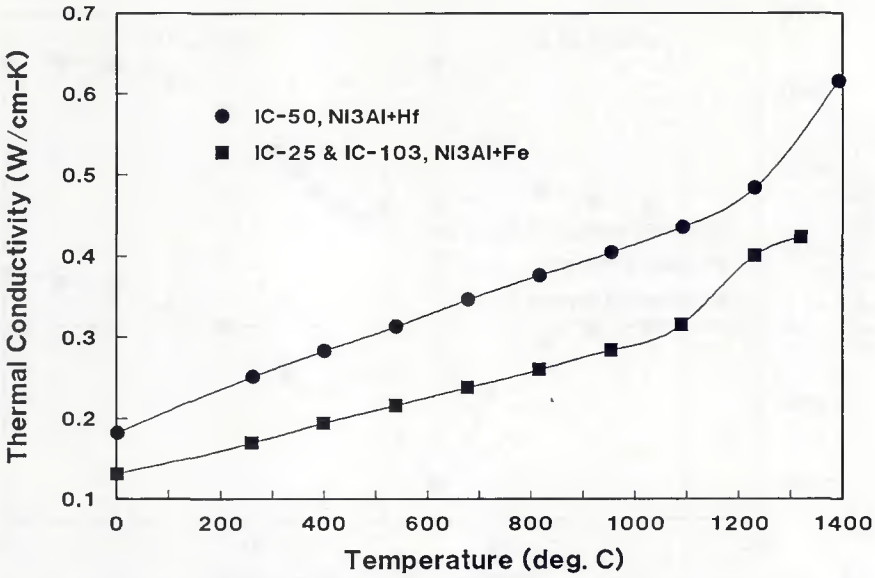

Fig. 9—Plot of thermal conductivity versus temperature for Ni_3Al+Fe and Ni_3Al+Hf alloys

Table 3—Electrical and Thermal Conductivities for Ni_3Al+Hf and Ni_3Al+Fe Alloys Studied

Temperature (°C)	Resistivity ($\mu\Omega$-cm) IC-50	Resistivity ($\mu\Omega$-cm) IC-25	Thermal Conductivity (W/cm-°K) IC-50	Thermal Conductivity (W/cm-°K) IC-25
0	64.0	92.0	0.183	0.131
260	75.4	117.6	0.252	0.169
399	80.0	121.6	0.284	0.194
538	84.0	126.0	0.315	0.216
677	86.7	129.6	0.347	0.238
812	89.0	131.9	0.377	0.260
954	92.0	133.1	0.405	0.284
1093	93.4	130.3	0.436	0.315
1232	90.5	107.8	0.485	0.400
1320	—	106.9	—	0.423
1390	75.4	—	0.617	—

Note: The conductivities of IC-25 and IC-103 were assumed to be identical.

these Ni_3Al alloys with their welding behaviors may be more complex. The ductility of boron-doped Ni_3Al can be dramatically influenced by the environment in which they are tested (Refs. 15, 16). For instance, Liu (Ref. 15) showed that the ductility of a Ni-23Al-0.5Hf-0.07B at.-% alloy tested at a strain rate of 3.3×10^{-3}/s increased from near zero to 25% as air pressure was reduced from 0.13 kPa to 1.3 μPa, and attributed the reduction in ductility at the higher air pressures to oxygen embrittlement. These findings suggest that our analysis may have two possible shortcomings: 1) the ductilities of the Ni_3Al Alloys IC-50, IC-25 and IC-103 shown in Fig. 2 were underestimated because the tests were done in air, and 2) the correlation of this ductility data with the welding observations is not valid because the welds were made in vacuum. These problems are currently being addressed by additional testing, and recent, unpublished results indicated that the ductility of the Ni_3Al+Hf Alloy IC-50 is not significantly affected by test environment at or above 800°C. Specifically, these results showed that for testing in vacuum at a strain rate of 3.2/s, IC-50 had only about 1% elongation at 800°C, and no measurable ductility above this temperature. Other data indicated that the ductility of IC-50 at 1000°C (1832°F) in vacuum and air increased only slightly at strain rates below 3.2/s. Consequently, we conclude that failing to account for environmental effects on ductility had no significant adverse effect on our correlation of hot-ductility data and welding behavior for the Ni_3Al alloys we studied, and would not cause conclusions based on these data to be invalidated. A report of additional work on effects of environment on ductility, and possible effects of strain rate on HAZ cracking of boron-doped Ni_3Al alloys will be made later.

Conclusion

The resistance to HAZ cracking of a Ni_3Al alloy containing 0.5 at.-% Hf and 0.1 at.-% B was found to be very good, although the alloy had no measurable ductility above 800°C. This result was inconsistent with a previous correlation of weldability and hot ductility made for boron-doped Ni_3Al alloys containing 10 at.-% Fe.

A computer-aided analysis of the transient longitudinal thermal stresses induced by welding was used to examine the problem of HAZ cracking of the Ni_3Al alloys in more depth. Computer generated thermal stress profiles were compared to the variation with temperature of the yield strengths of the two types of alloys. It was established that for the Ni_3Al+Hf alloy, the induced thermal stresses in the HAZ, σ_T, never exceeded the yield strength, σ_M. Thus, resistance to HAZ cracking was very good. It was concluded that relatively high thermal conductivity of the Ni_3Al+Hf alloy, as compared to the Ni_3Al+Fe alloys, was the major factor in the resistance of this alloy to HAZ cracking.

For the Ni_3Al+Fe alloys, the induced thermal stresses in the HAZ were predicted to exceed the yield strength under welding conditions where HAZ cracking was actually observed. Alloys such as IC-25, which had no measurable high-temperature ductility, cannot accommodate the high thermal stresses and are very susceptible to cracking. The good HAZ-cracking resistance of Ni_3Al+Fe Alloy IC-103 was attributed to its ability to accommodate thermal stresses in excess of the yield strength by local plastic flow.

Computer modeling of thermal stresses permitted the inconsistencies of the correlation between weldability and hot ductility to be resolved for the Ni_3Al alloys and resulted in a coherent explanation of HAZ-cracking behavior for these materials.

Appendix

Input data for temperature profile calculations—The physical property data required to calculate the temperature profiles for any given set of welding conditions were thermal conductivity, heat capacity and density. Accurate density measurements were available from the literature (Ref. 17) and it was assumed that any changes resulting from compositional variations and thermal expansion were negligible.

Heat capacity data for Ni_3Al were not available in the literature but were estimated using the Neumann-Kopp rule (Ref. 18), which can estimate for alloy phases with reasonable accuracy. By this method, the heat capacity of an alloy is the composition-weighted sum of the heat capacity for each individual elemental component. The heat capacities for the alloys were estimated as c_p,

$Ni_3Al = 0.75c_p$, $Ni + 0.25c_p$,Al. Allowing for the addition of iron to Ni_3Al had little effect on the estimated c_p value, so the same approximation was used for both types of alloys used in this study.

Thermal conductivity can be estimated from electrical conductivity via a phonon-corrected Wiedmann-Franz law that states:

$$\Gamma = LT/\beta + p_c \quad (2)$$

where,

L = Lorenz number = 2.45×10^{-8} W-Ω/°K^2
T = Absolute temperature, °K
β = Electrical resistivity, Ω-m
p_c = Phonon thermal conduction, W/m-°K

The approximation accounts mainly for thermal conduction from a degenerate electron gas. A small correction term was added for phonon conduction but this contribution becomes small at higher temperatures. Experimental data for the temperature variation at electrical conductivities of both the Ni_3Al+Hf and Ni_3Al+Fe alloys were available from published reports (Refs. 19, 20). The conductivity data take account of phase changes that occur at elevated temperature, and are presented in Table 3, and plotted in Fig. 9.

Input data for calculation of induced thermal stress profiles—The property data required for the calculation of the thermal stresses induced by welding were the variations of elastic modulus, yield strength, strain-hardening parameter and thermal expansion with temperature. Data for the variation of elastic modulus of Ni_3Al with temperature up to 850°C (1562°F) were available from the work of Dickson and coworkers (Ref. 21). Since the elastic modulus is relatively insensitive to composition, these data were used for the elastic moduli of both types of Ni_3Al alloys. No experimental data were available for temperatures above 850°C so the existing data were simply extrapolated up to the higher temperatures required for the thermal stress calculation and assumed to be zero at the melting points of the alloys. The variations of yield strength with temperature were taken from the work of Liu, *et al.* (Refs. 22, 23) for temperatures up to 900°C (1652°F) and were extrapolated to higher temperatures using data generated from our own hot-ductility testing. The yield strength data are plotted in Figs. 4 and 5.

A strain-hardening parameter, as defined by Masubuchi, *et al.* (Refs. 6, 7) has a value of unity in the elastic region of the stress-strain curve, and is less than one in the plastic region. A value of 0.1 (Ref. 24) was used for both types of Ni_3Al alloys between room temperature and the temperature at which the peak yield strength occurred. Above the temperature of the peak yield strength, the strain-hardening parameter was set equal to unity because the alloys were brittle above this point.

Thermal expansion data were taken from Williams, *et al.* (Ref. 19), and Stoeckinger and Neumann (Ref. 25). The effect of a 10 at.-% iron addition on the thermal expansion coefficient of Ni_3Al is not known, so the same values were used for both Ni_3Al+Fe and Ni_3Al+Hf alloys.

Acknowledgments

The authors wish to thank C. T. Liu for his technical support and review of the manuscript, and R. W. Swindeman for technical review of the manuscript. This research was sponsored jointly by the U.S. Department of Energy, Energy Conversion and Utilization Technologies (ECUT) Program, and the AR&TD Fossil Energy Program under contract DE-AC05-840R21400 with Martin-Marietta Energy Systems, Inc.

References

1. Aoki, K., and Izumi, D. 1979. *Nippon Kinzaku Gakkaishi* 43:1190.
2. Liu, C. T., White, C. L., and Horton, J. A. 1985. *Acta Metall.* 33:213.
3. David, S. A., Jemian, W. A., Liu, C. T., and Horton, J. A. 1985. *Welding Journal* 64(1):22-s to 28-s.
4. Santella, M. L., David, S. A., and White, C. L. 1985. *Proceedings of a Symposium on High-Temperature Ordered Intermetallic Alloys, November 1984.* Materials Research Society, pp. 495–503.
5. Santella, M. L., and David, S. A. 1986. *Welding Journal* 65(5): 129-s.
6. Masubuchi, K., Simmons, F. B., and Monroe, R. E. 1968. *Analysis of Thermal Stresses and Metal Movement during Welding.* RSIC-820, Redstone Scientific Information Center, Redstone Arsenal, Ala.
7. Andrews, J. B., Arita, M., and Masubuchi, K. 1970. *Analysis of Thermal Stress and Metal Movement during Welding.* NASA Contractor Report NASA CR-61351. G. C. Marshall Space Flight Center, Huntsville, Ala.
8. Rosenthal, D. 1941. *Welding Journal* 20(5): 220-s.
9. Tall, L. 1964. *Welding Journal* 43(1): 10-s.
10. Nippes, E. F., Savage, W. F., Bastian, B. J., Mason, H. F., and Curran, R. M. 1955. *Welding Journal* 34(4): 183-s.
11. Owczarski, W. A., Duvall, D. S., and Sullivan C. P. 1966. *Welding Journal* 45(4): 145-s.
12. Weiss, B., Grotke, G. E., and Strickler, R. 1970. *Welding Journal* 49(10): 471-s.
13. Masubuchi, K. 1980. *Analysis of Welded Structures.* Pergamon Press Inc., New York, N.Y.
14. Yeniscavich, W. 1970. *Proceedings of a Symposium on Methods of High-Alloy Weldability Evaluation.* Welding Research Council, pp. 2–12.
15. Liu, C. T. 1987. *Proceedings of a Symposium on High-Temperature Ordered Intermetallic Alloys, November 1986.* Materials Research Society, pp. 355–367.
16. Liu, C. T. and White, C. L. *Acta Metall.* 35(3): 643–649.
17. Williams, R. K., Graves, R. S., and Weaver, F. J. *J. Appl. Phys.* 61(4): 1486–1492.
18. Kubaschewski, O., and Alcock, C. B. 1979. *Metallurgical Thermochemistry.* Pergamon Press, Inc., Elmsford, N.Y. pp. 179–185.
19. Williams, R. K., Graves, R. S., Weaver, F. J., and McElroy, D. L. 1985. *High-Temperature Ordered Intermetallic Alloys.* Materials Research Society, Pittsburgh, Pa., pp. 505–512.
20. Schneider, J. S. 1986. *Effects of Temperature and Composition on the Electrical Resistivity and Long-Range Order of Ni_3Al.* ORNL/CF-86/369, Oak Ridge National Laboratory, Oak Ridge, Tenn.
21. Dickson, R. W., Wachtman, J. B., and Copley, S. M. 1966. *J. Appl. Phys.* 40(5): 2276–2279.
22. Liu, C. T., White, C. L., Koch, C. C., and Lee, E. H. 1983. *Proceedings of the Symposium on High-Temperature Materials Chemistry II.* Munir and Cubicciotti, ed., The Electrochemical Society, Inc.
23. Liu, C. T., Jemian, W., Inouye, H., Cathcart, J. V., David, S. A., Horton, J. A., and Santella, M. L. 1984. *Initial Development of Nickel and Nickel-Iron Aluminides for Structural Uses.* ORNL-6067, Oak Ridge National Laboratory, Oak Ridge, Tenn.
24. Aoki, K., and Izumi, O. 1978. *Trans. JIM* 19: 203–210.
25. Stoeckinger, G. R., and Neumann, J. P. 1970. *J. Appl. Cryst.* 3: 32–38.